Near-zero anomalous dispersion $Ge_{11.5}As_{24}Se_{64.5}$ glass nanowires for correlated photon pair generation: design and analysis

X. Gai,[1,*] R. P. Wang,[1] C. Xiong,[2] M. J. Steel,[3] B. J. Eggleton,[2] and B. Luther-Davies[1]

[1]*Centre for Ultrahigh-bandwidth Devices for Optical Systems (CUDOS), Laser Physics Centre, Research School of Physics and Engineering, The Australian National University, Canberra ACT2600, Australia*
[2]*CUDOS, Institute of Photonics and Optical Science (IPOS), School of Physics, University of Sydney, NSW 2006 Australia*
[3]*CUDOS, MQ Photonics Research Centre, Department of Physics and Astronomy, Faculty of Science, Macquarie University, NSW 2109 Australia*
[*]*xga111@rsphysse.anu.edu.au*

Abstract: We show that highly nonlinear chalcogenide glass nanowire waveguides with near-zero anomalous dispersion should be capable of generating correlated photon-pairs by spontaneous four-wave mixing at frequencies detuned by over 17 THz from the pump where Raman noise is absent. In this region we predict a photon pair correlation of >100, a figure of merit >10 and brightness of ~8×10^8 pairs/s over a bandwidth of >15 THz in nanowires with group velocity dispersion of <5 ps·km^{-1}nm^{-1}. We present designs for double-clad $Ge_{11.5}As_{24}Se_{64.5}$ glass nanowires with realistic tolerance to fabrication errors that achieve near-zero anomalous dispersion at a 1420 nm pump wavelength. This structure has a fabrication tolerance of 80–170 nm in the waveguide width and utilizes a SiO_2/Al_2O_3 layer deposited by atomic layer deposition to compensate the fabrication errors in the film thickness.

OCIS codes: (130.2755) Glass waveguides; (190.4380) Nonlinear optics, four-wave mixing; (270.4180) Multiphoton processes.

References and links

1. N. Yoran and B. Reznik, "Deterministic linear optics quantum computation with single photon qubits," Phys. Rev. Lett. **91**(3), 037903 (2003).
2. N. Gisin, G. Ribordy, W. Tittel, and H. Zbinden, "Quamtum cryptography," Rev. Mod. Phys. **74**(1), 145–195 (2002).
3. J. C. F. Matthews, A. Politi, A. Stefanov, and J. L. O'Brien, "Manipulating multi-photon entanglement in waveguide quantum circuits," Nat. Photonics **3**(6), 346–350 (2009).
4. X. Li, J. Chen, P. Voss, J. Sharping, and P. Kumar, "All-fiber photon-pair source for quantum communications: Improved generation of correlated photons," Opt. Express **12**(16), 3737–3744 (2004).
5. J. E. Sharping, K. F. Lee, M. A. Foster, A. C. Turner, B. S. Schmidt, M. Lipson, A. L. Gaeta, and P. Kumar, "Generation of correlated photons in nanoscale silicon waveguides," Opt. Express **14**(25), 12388–12393 (2006).
6. A. D. Bristow, N. Rotenberg, and H. M. van Driel, "Two-photon absorption and Kerr coefficients of silicon for 850–2200 nm," Appl. Phys. Lett. **90**(19), 191104 (2007).
7. M. R. Lamont, B. Luther-Davies, D.-Y. Choi, S. Madden, X. Gai, and B. J. Eggleton, "Net-gain from a parametric amplifier on a chalcogenide optical chip," Opt. Express **16**(25), 20374–20381 (2008).
8. F. Luan, M. D. Pelusi, M. R. E. Lamont, D.-Y. Choi, S. Madden, B. Luther-Davies, and B. J. Eggleton, "Dispersion engineered As_2S_3 planar waveguides for broadband four-wave mixing based wavelength conversion of 40 Gb/s signals," Opt. Express **17**(5), 3514–3520 (2009).
9. C. Xiong, G. D. Marshall, A. Peruzzo, M. Lobino, A. S. Clark, D.-Y. Choi, S. J. Madden, C. M. Natarajan, M. G. Tanner, R. H. Hadfield, S. N. Dorenbos, T. Zijlstra, V. Zwiller, M. G. Thompson, J. G. Rarity, M. J. Steel, B. Luther-Davies, B. J. Eggleton, and J. L. O'Brien, "Generation of correlated photon pairs in a chalcogenide As_2S_3 waveguide," Appl. Phys. Lett. **98**(5), 051101 (2011).
10. C. Xiong, L. G. Helt, A. C. Judge, G. D. Marshall, M. J. Steel, J. E. Sipe, and B. J. Eggleton, "Quantum-correlated photon pair generation in chalcogenide As_2S_3 waveguides," Opt. Express **18**(15), 16206–16216 (2010).

#154945 - $15.00 USD Received 19 Sep 2011; revised 21 Nov 2011; accepted 23 Nov 2011; published 3 Jan 2012

11. A. S. Y. Hsieh, G. K. L. Wong, S. G. Murdoch, S. Coen, F. Vanholsbeeck, R. Leonhardt, and J. D. Harvey, "Combined effect of Raman and parametric gain on single-pump parametric amplifiers," Opt. Express **15**(13), 8104–8114 (2007).
12. G. P. Agrawal, *Nonlinear Fiber Optics*, 3rd. ed. (Academic, 2001).
13. A. Prasad, C.-J. Zha, R.-P. Wang, A. Smith, S. Madden, and B. Luther-Davies, "Properties of $Ge_xAs_ySe_{1-x-y}$ glasses for all-optical signal processing," Opt. Express **16**(4), 2804–2815 (2008).
14. X. Gai, S. Madden, D.-Y. Choi, D. Bulla, and B. Luther-Davies, "Dispersion engineered $Ge_{11.5}As_{24}Se_{64.5}$ nanowires with a nonlinear parameter of 136 $W^{-1}m^{-1}$ at 1550 nm," Opt. Express **18**(18), 18866–18874 (2010).
15. X. Gai, T. Han, A. Prasad, S. Madden, D.-Y. Choi, R. Wang, D. Bulla, and B. Luther-Davies, "Progress in optical waveguides fabricated from chalcogenide glasses," Opt. Express **18**(25), 26635–26646 (2010).
16. S. M. George, "Atomic Layer Deposition: An Overview," Chem. Rev. **110**(1), 111–131 (2010).
17. X. Gai, D.-Y. Choi, S. Madden, and B. Luther-Davies, "Interplay between Raman scattering and four-wave mixing in As_2S_3 chalcogenide glass waveguides," J. Opt. Soc. Am. B **28**(11), 2777–2784 (2011).
18. Q. Lin, J. Zhang, P. M. Fauchet, and G. P. Agrawal, "Ultrabroadband parametric generation and wavelength conversion in silicon waveguides," Opt. Express **14**(11), 4786–4799 (2006).
19. A. B. Fallahkhair, K. S. Li, and T. E. Murphy, "Vector finite-difference mode solver for anisotropic dielectric waveguides," J. Lightwave Technol. **26**(11), 1423–1431 (2008).
20. P. Lüsse, P. Stuwe, J. Schüle, and H. G. Unger, "Analysis of vectorial mode fields in optical waveguides by a new finite difference method," J. Lightwave Technol. **12**(3), 487–494 (1994).

1. Introduction

Quantum-correlated photon pairs can serve as either a source of entangled photons or a heralded single-photon source both of which are critical for applications such as linear optical quantum computing, quantum cryptography, and integrated optical quantum devices [1–3]. Recently, spontaneous four-wave mixing (SFWM) has attracted a lot of attention as a natural way to generate correlated photon pairs due to its potential for higher efficiency and compatibility with integrated devices. Correlated photon pairs based on SFWM have been generated in silica fibers [4] and silicon waveguides [5]. However, the low nonlinear index of silica limits its application for on-chip integration. Silicon has better performance in terms of nonlinear refractive index, but its strong two-photon absorption (TPA) and free carrier absorption (FCA) degrade the device performance [6]. In comparison, As_2S_3 chalcogenide glasses has been reported to have >100 times the nonlinearity of silica and negligible TPA and FCA suggesting they are a good platform for photonic integrated circuits [7,8]. Recently correlated photon pairs were generated in As_2S_3 waveguides by SFWM [9,10]. However, as a glass, the correlated photon pairs generated in As_2S_3 waveguides also experienced spontaneous Raman scattering (SpRS) that limited the degree of quantum correlation. Some strategies were suggested to overcome this limitation [10] e.g., using the low Raman gain windows in the As_2S_3 SpRS spectrum at a frequency shift of about 7.4 THz or by using engineered dispersion and reduced waveguide length to extend the FWM bandwidth to large frequency shifts beyond the range of SpRS.

The latter solution is interesting because it would lead to photon pair generation in a spectral region where SpRS is essentially absent. However, there are significant challenges when fabricating devices to implement this approach. Firstly, SpRS not only leads to noise via the imaginary part of the Raman response function that contributes to SpRS gain, but also modulates the effective nonlinearity which drives SFWM because of the influence of the large negative real part of the Raman response function on the high frequency side of the SpRS gain curve [11,12]. This has the effect of reducing the pair generation rate and thus increasing the frequency shift needed to avoid SpRS which in turn means that even smaller anomalous dispersion is required. This is a real challenge because of the high sensitivity of dispersion to the waveguide dimensions. The need for very small dispersion can be alleviated somewhat by using short waveguides which reduce the total device dispersion. However, in order to obtain adequate SFWM efficiency the waveguides must then have a very high nonlinear parameter, such as that only obtainable by using nanowires with sub-wavelength transverse dimensions. As a result, nanowires made from a material with a high nonlinearity, a low SpRS detuning frequency and negligible TPA and FCA are required to generate correlated photon pairs in glass waveguides at frequencies where SpRS noise can be avoided. The structure must then be

#154945 - $15.00 USD Received 19 Sep 2011; revised 21 Nov 2011; accepted 23 Nov 2011; published 3 Jan 2012

designed for almost zero anomalous dispersion and importantly must have a high tolerance to fabrication errors to be manufacturable.

Recently, $Ge_{11.5}As_{24}Se_{64.5}$ ($Ge_{11.5}$) chalcogenide glass has been reported with a nonlinear refractive index 3 times higher than that of As_2S_3 with negligible TPA and FCA [13]. This material has been used to fabricate glass nanowire waveguides with a nonlinear parameter as high as 140 $W^{-1}m^{-1}$ at 1550 nm and moderate losses of ≈1.5 dB/cm in the fundamental TM mode [14,15]. Such a high nonlinearity allows high SFWM efficiency to be obtained in a short length (<1 cm) somewhat reducing the limitation on the dispersion. Furthermore, $Ge_{11.5}As_{24}Se_{64.5}$ glass has a significantly narrower SpRS detuning frequency compared with As_2S_3 due to the substitution of higher mass Se atoms for S in the glass matrix. This suggests it is a better choice for generating correlated photon pairs at frequencies beyond the SpRS noise.

In this paper, we have analyzed correlated photon pair generation in $Ge_{11.5}$ nanowire waveguides as a function of detuning from the pump frequency. Our analysis includes the effects of dispersion, nonlinearity and both the real and imaginary parts of response function for SpRS. We show that the best figure of merit, defined as the ratio of pair generation rate from SFWM to the noise generated by SpRS, is achieved for frequency shifts greater than 17 THz above the pump. In this region a photon pair correlation >100 is achievable in theory, together with a figure of merit >10 at a pair generation rate $>8 \times 10^8$ pairs/s.

In order to access this region we have developed designs for $Ge_{11.5}$ nanowires with near-zero anomalous dispersion for the fundamental TM mode that have a high tolerance to fabrication errors. Because the nonlinear parameter of these nanowires is large, a short waveguide can be used, which means the GVD needs to lie between zero and 7 $ps \cdot km^{-1}nm^{-1}$ as we discuss later. Since it is important that the correlated photons are generated at frequencies where high detection efficiency is available from an InGaAs single photon detector, the pump wavelength was chosen to be 1420 nm and this leads to the generation of photon pairs at wavelengths of 1314 nm (signal) and 1544 nm (idler).

From our analysis of the waveguide design, we found that low dispersion $Ge_{11.5}$ nanowires can have a high tolerance to errors in the waveguide width, but are then very sensitive to waveguide thickness. As a result, we developed a cladding design that uses a dual-layer to compensate for fabrication errors in the waveguide thickness. This design employs a thin layer of SiO_2 or Al_2O_3 between the waveguide and a top cladding with a refractive index of 1.52. The implementation requires the exact waveguide thickness to be determined post fabrication using highly accurate metrology, such as optical profilometry, with nm precision. The dual layer cladding then allows the GVD to be tuned to become near-zero by depositing a layer whose thickness can be controlled with high accuracy using a process such as atomic layer deposition (ALD) [16].

2. Correlated photon-pair generation with CW pump

In order to analyze the quality of correlated photon-pair generation by SFWM in $Ge_{11.5}$ nanowires, we need to treat the influence of SpRS on the SFWM carefully because this contributes not only Raman gain, arising from the imaginary part of Raman response function, but also affects the nonlinear phase modulation for SFWM via the real part of the response function [11,17]. As very low pump power is used for correlated photon pair generation, the undepleted pump approximation can be used in the analysis. In addition, the power of idler has a negligible influence on the pump. We, therefore, deduced Eqs. (1), (2) and (3) shown below from Refs. [11,17,18] and these describe the interaction between the pump, signal and idler including SpRS:

#154945 - $15.00 USD Received 19 Sep 2011; revised 21 Nov 2011; accepted 23 Nov 2011; published 3 Jan 2012

$$\frac{\partial A_p}{\partial z}+\frac{i}{2}\beta_2\frac{\partial^2 A_p}{\partial t^2}+\frac{\alpha}{2}A_p$$
$$=i\gamma\left[\left|A_p\right|^2+(2+f_R(\mathrm{Re}\left[\tilde{h}_R(-\Omega)\right]-1))\left|A_s\right|^2+(2+f_R(\mathrm{Re}\left[\tilde{h}_R(\Omega)\right]-1))\left|A_i\right|^2\right]A_p \quad (1)$$
$$-\gamma\,\mathrm{Im}\left[\tilde{h}_R(-\Omega)\right]f_R\left|A_s\right|^2A_p-\gamma\,\mathrm{Im}\left[\tilde{h}_R(\Omega)\right]f_R\left|A_i\right|^2A_p,$$

$$\frac{\partial A_s}{\partial z}+\frac{i}{2}\beta_2\frac{\partial^2 A_s}{\partial t^2}+\frac{\alpha}{2}A_s=i\gamma\left[\left|A_s\right|^2+(2+f_R(\mathrm{Re}\left[\tilde{h}_R(\Omega)\right]-1))\left|A_p\right|^2\right]A_s$$
$$+i\gamma\left[1+f_R(\mathrm{Re}\left[\tilde{h}_R(\Omega)\right]-1)\right]A_p^2A_i^* \quad (2)$$
$$-\gamma\,\mathrm{Im}\left[\tilde{h}_R(\Omega)\right]f_R\left|A_p\right|^2A_s-\gamma\,\mathrm{Im}[\tilde{h}_R(\Omega)]f_RA_p^2A_i^*,$$

$$\frac{\partial A_i}{\partial z}+\frac{i}{2}\beta_2\frac{\partial^2 A_i}{\partial t^2}+\frac{\alpha}{2}A_i=i\gamma\left[\left|A_i\right|^2+(2+f_R(\mathrm{Re}\left[\tilde{h}_R(-\Omega)\right]-1))\left|A_p\right|^2\right]A_i$$
$$+i\gamma\left[1+f_R(\mathrm{Re}\left[\tilde{h}_R(-\Omega)\right]-1)\right]A_p^2A_s^* \quad (3)$$
$$-\gamma\,\mathrm{Im}\left[\tilde{h}_R(-\Omega)\right]f_R\left|A_p\right|^2A_i-\gamma\,\mathrm{Im}[\tilde{h}_R(-\Omega)]f_RA_p^2A_s^*,$$

Here the subscripts p, s and i refer to the pump, signal, and idler, respectively; $\Omega = \omega_s$-ω_p is the frequency detuning from signal to pump; β_2 is the second order dispersion; α is the linear loss, γ is the nonlinear parameter; $f_R = 0.13$ is fractional Raman factor of $Ge_{11.5}$; and $h_R(\Omega)$ is the Fourier transform of the Raman response function $h_R(t)$. From examination of Eqs. (1), (2) and (3), we find that Im[$h_R(\Omega)$] appears in real part of the equation and contributes a term representing loss or gain and thus determines the production of SpRS noise during the generation of correlated photon pairs. At the same time, the term containing Re[$h_R(\Omega)$] contributes to the imaginary part of the equation and modifies the nonlinear coefficient for cross-phase modulation (XPM) and energy conversion between the pump, signal and idler waves. The SFWM efficiency depends not only on the phase mismatch term between the propagation constants of the pump, signal and idler waves, but also on the effects of self-phase modulation [SPM] and XPM. As a result, we need to treat Re[$h_R(\Omega)$] carefully in SFWM whilst Im[$h_R(\Omega)$] is not so critical as it contributes to Raman gain appearing in all of the terms affecting SFWM. Furthermore, the phase matching condition for SFWM no longer contains only the dispersion and nonlinear parameters but also the real part of Raman function Re[$h_R(\Omega)$]. Thus, the phase matching condition which can be directly deduced from Ref. [11] has the form

$$-4\gamma P_0-4\gamma P_0 f(\mathrm{Re}[h_R(\omega)]-1)<2\beta_2\Delta\omega^2<0. \quad (4)$$

In Fig. 1, we plot Im[$h_R(\Omega)$] and Re[$h_R(\Omega)$] for $Ge_{11.5}$, As_2S_3 and silica deduced from the Raman gain spectrum for these materials via the Kramers-Kronig relations. The Raman gain spectrum of $Ge_{11.5}$ and As_2S_3 were measured by Raman spectroscopy whilst that for SiO_2 was obtained from Ref. [12]. The main peak of Im[$h_R(\Omega)$] for $Ge_{11.5}$ has the lowest frequency shift of these three materials making it the best choice for photon pair generation using SFWM in a region of the spectrum beyond the Raman peak where SpRS noise should be absent. In addition, there are large negative values of Re[$h_R(\Omega)$] for all three materials which decrease the SFWM conversion efficiencies at detunings just beyond the Raman gain peak. However Re[$h_R(\Omega)$] for $Ge_{11.5}$ recovers at the lowest detuning and thus offers the greatest potential for broad bandwidth SFWM beyond ≈10 THz.

#154945 - $15.00 USD Received 19 Sep 2011; revised 21 Nov 2011; accepted 23 Nov 2011; published 3 Jan 2012

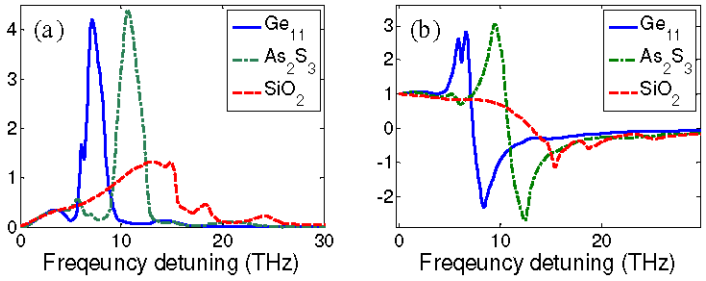

Fig. 1. Fourier transform of the Raman response function h_R of $Ge_{11.5}$, As_2S_3 and SiO_2. (a) The imaginary part Im[$h_R(\Omega)$]. (b) The real part Re[$h_R(\Omega)$].

As mentioned above, SFWM in $Ge_{11.5}$ nanowires involves not only the phase mismatch and the nonlinear phase modulation, but also the real part of Raman response function Re[$h_R(\Omega)$]. Thus the expression for the spectral density of the photon flux $G_i(\upsilon)$ should include Re[$h_R(\Omega)$] and can be calculated according to [11]:

$$G_i(\upsilon) = \frac{P_i(z)}{P_s(z)} = \left| \frac{q}{K - q - (iR)/\tanh(rRPL)} \right|^2, \tag{5}$$

where $R = \sqrt{K(2q-K)}$; $q(\Omega) = 1 - f_R + f_R\mathrm{Re}[h_R(\Omega)]$; K = $-\Delta k/(2\gamma P)$ is the ratio of the phase mismatch term arising from dispersion to the nonlinear term; $\Delta k(\Omega) = \beta_2\Omega^2 + \beta_4\Omega^4/12$, where β_4 is the fourth order dispersion of the waveguide; and where $\gamma \approx 140$ $W^{-1}m^{-1}$ for a $Ge_{11.5}$ nanowire [14]. The waveguide length L was chosen to be 0.5 cm because of the very high value of γ can supply enough nonlinearity in this short length for photon-pair generation. In addition, such a short waveguide also leads to broader SFWM bandwidth for the same dispersion.

The photon pair generation rate can be calculated according to [10] as $S_{SFWM}(\upsilon) \approx \Delta\upsilon \cdot G_i(\upsilon)$ where $\upsilon = \Omega/2\pi$ is the frequency detuning. We chose $\Delta\upsilon \approx 0.12$ THz corresponding to a 1 nm wide band-pass filter.

Shown in Fig. 2 is the calculated photon generation rate (PGR) for pure SFWM and SFWM including Re[$h_R(\Omega)$] with different values of GVD of 15, 5 and 1.5 ps·km^{-1}nm^{-1} and $\gamma PL = 0.1$ ($P \approx 0.14$ W). From Fig. 2, we can see that below 5 THz pure SFWM and SFWM including Re[$h_R(\Omega)$] have similar PGR. This is because Re[$h_R(\Omega)$]≈1 in this region as shown in Fig. 1(b). Between 5 and 7.5 THz, there is a dramatic increase in PGR because Re[$h_R(\Omega)$] increases in this region and this enhances the nonlinear phase modulation. From 7.5 to 12 THz, Re[$h_R(\Omega)$] becomes large and negative which reduces the nonlinear phase modulation leading to a dramatic decrease in the PGR. Beyond 12 THz Re[$h_R(\Omega)$] recovers towards zero and remains constant for higher frequencies. The PGR spectrum becomes flat at a level of 66%–75% of the PGR obtained from pure SFWM. This region has very small Raman noise according to Fig. 1(a) and thus has great potential as a source of correlated photon pairs. The bandwidth over which the PGR spectrum remains flat is mainly controlled by the waveguide dispersion. With GVD of 1.5, 5 and 15 ps·km^{-1}nm^{-1}, the bandwidth is ≈30, 20 and 8 THz respectively. This indicates the importance of obtaining near-zero anomalous dispersion to achieve correlated photon pairs at frequencies beyond the Raman noise. We choose the 5 ps·km^{-1}nm^{-1} GVD in the following calculations as a value that is realistic for the double clad dispersion engineered waveguides discussed later.

In order to analyze the quality of the correlated photon pair source we need to calculate the spectral density of the photon flux originating from Raman gain as this is the main noise source when generating correlated photon pairs by SFWM. The spectral density of the Raman

#154945 - $15.00 USD Received 19 Sep 2011; revised 21 Nov 2011; accepted 23 Nov 2011; published 3 Jan 2012

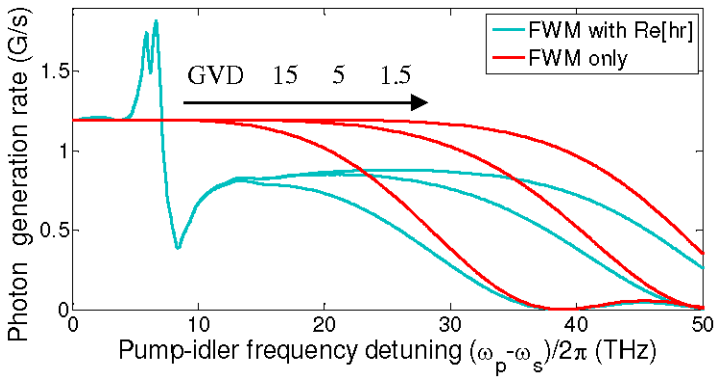

Fig. 2. Photon pair generation rate with γPL = 0.1 and GVD of 15, 5 and 1.5 ps·km^{-1}nm^{-1}Blue curve is for SFWM including Re[$h_R(\Omega)$]. Red curve is for pure SFWM. The frequency detuning is for pump-idler detuning ω_i-ω_p = ω_p-ω_s. G/s is for 1 × 10^9 pairs per second.

photon flux can be calculated according to [10] as

$$f_{SpRS} = PL\left|g_R(\upsilon)\right|(n_{th}+1), \tag{6}$$

where $g_R(\upsilon) = 2\gamma f_R \mathrm{Im}[h_R(2\pi\upsilon)]$ is the Raman gain spectrum of $Ge_{11.5}$; $n_{th} = 1/\exp(h\upsilon/k_BT) - 1$ is photon population at frequency υ and temperature T following the Bose-Einstein distribution; h is the Planck's constant; k_B is the Boltzmann constant; and the photon generation rate $S_{SpRS}(\upsilon)\approx\Delta\upsilon\cdot f_{SpRS}(\upsilon)$ where $\Delta\upsilon\approx0.12$ THz corresponds to a 1 nm band-pass filter. Another important criterion related to the quality of the correlated photon pair source is the figure of merit F which is defined by comparing the PGR from SFWM (signal) to PGR from SpRS (noise) as

$$F = \frac{S_{FWM}}{S_{SpRS}}. \tag{7}$$

In addition, uncorrelated photons due to multi-pair generation at high power stop us from improving the PGR and F by increasing the power. Assuming ideal filters are used for the signal and idler and pair correlation this can be calculated according to [10] as

$$\rho_{Raman} = \frac{[\gamma\,\mathrm{Re}(\eta)]^2 + \left|g_R(n_{th}+1/2)\right|^2}{[\left|\gamma\eta\right|^2 PL + \left|g_R(n_{th}+1)\right|][\left|\gamma\eta\right|^2 PL + \left|g_R\right|n_{th}]}, \tag{8}$$

where $\eta = 1\text{-}f_R + f_R h_R(\Omega)$.

Figure 3 shows the PGR of SFWM and Raman noise, the figure of merit and pair correlation at γPL of 0.07, 0.1 and 0.15 respectively. From Figs. 3 (b) and (c), we find that the figure of merit and pair correlation show opposite trends as a function of γPL since higher γPL values lead to stronger photon pair brightness but also increases the generation of uncorrelated multiple photon pairs. As a result, we focus on γPL = 0.1 as a compromise between the figure of merit and photon pair correlation. Because photons generated from Raman gain are the main noise source in our system, we can identify four interesting regions where Raman noise is relatively low. Region A lies below 0.4 THz. The PGR of SFWM in this region is the same as pure SFWM at about 1.2 G/s because Re[$h_R(\Omega)$] ≈1 as indicated above. The figure of merit and the pair correlation are ≈10 and ≈80 at maximum but drop rapidly below 5 and 60 for just by 0.3 THz frequency shift. Region B is the first low Raman gain window extending from 4.5 THz to 5.5 THz. This region has the highest SFWM PGR as the high value of Re[$h_R(\Omega)$] enhances the nonlinear phase modulation in this region but the figure of merit and pair

#154945 - $15.00 USD Received 19 Sep 2011; revised 21 Nov 2011; accepted 23 Nov 2011; published 3 Jan 2012

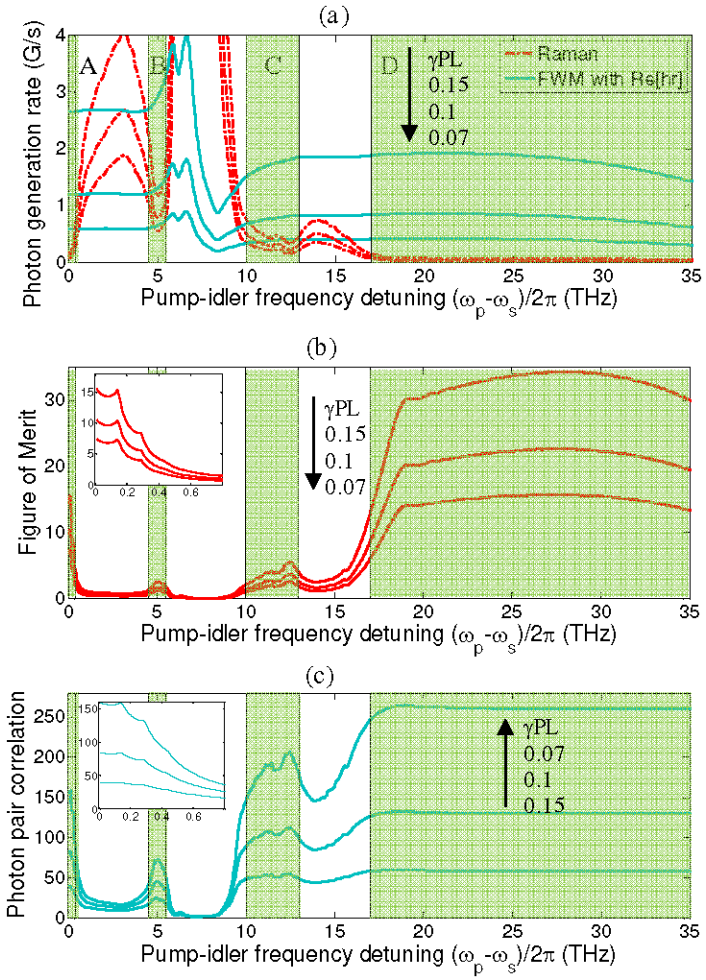

Fig. 3. Criteria for correlated photon pair generation for γPL = 0.07, 0.1 and 0.15. (a) The photon pair generation rate of SFWM and SpRS. (b) Figure of merit $F = S_{SFWM}/S_{SpRS}$. (c) Photon pair correlation. G/s is for 1×10^9 pairs per second.

correlation is only about 2.5 and 50 at maximum. Region C is the second low Raman gain window between 10 and 13 THz. The SFWM PGR has recovered from the dip of large negative values of Re[$h_R(\Omega)$] and remains constant at 0.8–0.9 G/s. The figure of merit is of 5 at maximum while the pair correlation is about 100 and remains constant in the region. Region D is defined between 17 THz and 35 THz. In this region, the PGR remains at 0.9 G/s over more than 15 THz bandwidth. The highest figure of merit and photon correlation is achieved here, the values being 20 and 130 respectively, and these remain constant across the whole detuning range. Region D is only accessible using ultra-low dispersion waveguide design and gives us a broad bandwidth photon pair source with best quality for a glass waveguide. Accessing this region, however, places the most demanding restrictions on dispersion and hence waveguide design.

3. Near-zero anomalous dispersion waveguides

In order to produce a design for a nanowire with near-zero anomalous dispersion with a high tolerance to fabrication errors, we need to firstly consider the fabrication process and identify where the main errors occur. Figure 4(a) shows a standard waveguide structure and its refractive index profile. In the fabrication process a $Ge_{11.5}$ film is deposited onto an oxidized

#154945 - $15.00 USD Received 19 Sep 2011; revised 21 Nov 2011; accepted 23 Nov 2011; published 3 Jan 2012

silicon wafer by thermal evaporation at a rate ~0.2–0.3 nm/s to a thickness of 500–650 nm with an uncertainty of ~±10–15 nm. The precise film thickness can be measured after deposition to better accuracy (±5 nm) using a dual angle spectroscopic reflectometer (SCI Filmtek 4000) or post etching with an optical profiler to an accuracy of ±2 nm. The width of the waveguides is determined by the lithography and etching processes. In those processes the waveguides are first patterned onto 250 nm ZEP by electron-beam lithography (EBL) with 20 µm aperture and 30 kV acceleration voltage. The fixed beam moving stage (FBMS) method was applied to remove all the stitching errors between different write-fields. Following this inductively coupled plasma etching is used to transfer the waveguide patterns into the $Ge_{11.5}$ films. At the end of process, an inorganic polymer glass (IPG) is spin-coated onto the waveguides as a top cladding with a refractive index of 1.52 at 1420 nm. During fabrication, the widths of waveguides can vary from the design values due to errors in the pattern width introduced during EBL and due to process bias during ICP etching. These create an uncertainty of ~±15–20 nm in the waveguide width. Hence the fabrication errors that affect dispersion arise from errors in both the thickness of the deposited film and the width of the nanowires.

In previous work, the waveguide dispersion was designed by varying the film thickness assuming the waveguide width was known. Under this assumption, we calculated the GVD for a 0.625 µm wide $Ge_{11.5}$ waveguide as a function of film thickness using the finite difference method [19,20].

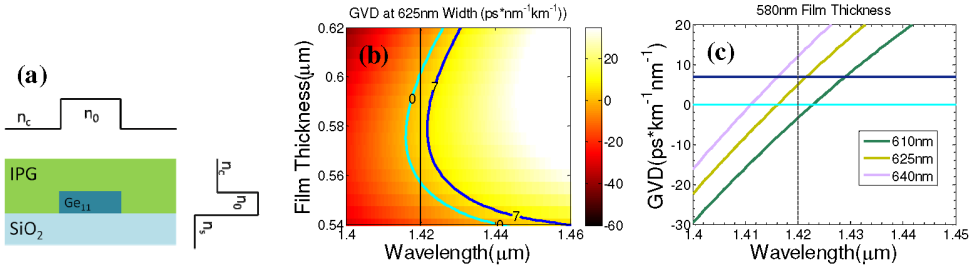

Fig. 4. (a) A standard single clad $Ge_{11.5}$ waveguide structure. (b) The GVD for a 0.625 µm wide waveguide. Dark blue curve is the contour for GVD of 7 ps·km^{-1}nm^{-1}; light blue curve is the zero-dispersion contour; the black line shows the pump wavelength at 1.42 µm. (c) the GVD for a 0.58 µm film thickness and 0.61, 0.625 and 0.64 µm waveguide width.

The results are shown in Fig. 4(b) where the vertical black line indicates a wavelength of 1420 nm and the light and dark blue curves are the contours for zero-dispersion and a GVD of 7 ps·km^{-1}nm^{-1} respectively. From Fig. 4(b), we find that the zero-dispersion contour intercepts the 1420nm line at thicknesses of 0.56 and 0.6 µm and the maximum GVD is 5 ps·km^{-1}nm^{-1} at 1420 nm at a thickness of 0.58 µm. This shows that if there was no error in the waveguide width, the tolerance on film thickness is ±20 nm and this is larger than the ±15 nm fabrication tolerance associated with film deposition making a GVD < 5 ps·km^{-1}nm^{-1} achievable.

In order to analyze whether such structure is practical, we studied the tolerance to fabrication errors in the waveguide width for this structure and this is shown in Fig. 4(c). Figure 4(c) plots the GVD of 0.58 µm thick waveguides with different widths of 0.61, 0.625 and 0.64 µm respectively and shows that with +15 nm fabrication error on waveguide width, the GVD has increased up to 12 ps·km^{-1}nm^{-1} at 1420 nm exceeding the requirement of a maximum GVD of 7 ps·km^{-1}nm^{-1}. With the −15 nm fabrication error, the GVD decreased to −3.5 ps·km^{-1}nm^{-1} breaking the requirement for anomalous dispersion. Since ±20 nm errors can result from the fabrication process this structure shows poor tolerance to errors in the waveguide width making it difficult to achieve low and predictable anomalous dispersion.

#154945 - $15.00 USD Received 19 Sep 2011; revised 21 Nov 2011; accepted 23 Nov 2011; published 3 Jan 2012

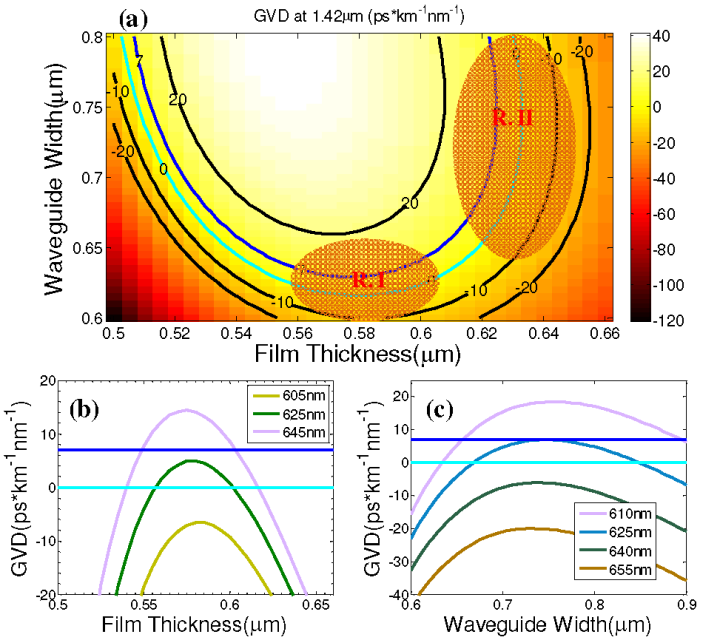

Fig. 5. (a) GVD at 1.42 μm as a function of film thickness and waveguide width. (b) GVD as a function of film thickness in region I. (c) GVD as a function of waveguide width in region II.

As a result, to identify a structure with better tolerance to fabrication errors, we have to study the GVD as a function of both waveguide width and thickness. This is shown in Fig. 5(a). Here the dark and light blue curves indicate 7 ps·km^{-1}nm^{-1} and zero dispersion respectively and black curves are for 20, −10 and −20 ps·km^{-1}nm^{-1} as indicated. From Fig. 5(a), there are two regions of interest. Region I is located at film thicknesses between 0.56 and 0.6 μm and waveguide width between 0.6 and 0.65 μm. In this region, we observed a slow dependence of GVD on film thickness. More details are shown in Fig. 5(b), where for the 0.625 μm wide waveguide, a >40 nm change in film thickness from 0.56 to 0.6 μm leads to only 5 ps·km^{-1}nm^{-1} variation on GVD from 0 to 5 ps·km^{-1}nm^{-1}. In fact, this is the same structure as studied in Fig. 4 that was very sensitive to waveguide width. However, an interesting observation from Fig. 5(b) is that the GVD curves contain a local maximum and their shape is only weakly dependent on width, although the maximum GVD value shifts quite rapidly. This presence of this local maximum explains the insensitivity to film thickness and results in the GVD varying by <7 ps·km^{-1}nm^{-1} from the peak value for >50 nm change in thickness.

The second interesting region II has similar features, but this time the GVD varies only slowly with waveguide width. According to Figs. 5(a) and 5(c), we find that for a film thickness of 0.625 μm, the GVD varies between zero and 7 ps·km^{-1}nm^{-1} for a 170 nm change in waveguide width from 0.67 to 0.85 μm. The tolerance to waveguide width is much larger than the estimated fabrication errors making them negligible. However, the GVD is now sensitive to film thickness as shown in Fig. 5(c), where the peak GVD for a 0.61 μm wide waveguide increases to 18 ps·km^{-1}nm^{-1} and that for the 0.64 μm wide waveguide decreased to −6 ps·km^{-1}nm^{-1} which is far larger than can be tolerated. As was the case of Fig. 5(b) the existence of a local maximum explains the insensitivity to width and all structures have over 170 nm tolerance to waveguide width for <7 ps·km^{-1}nm^{-1} variation from the peak value of GVD. Region II is of more interest because of its much bigger tolerance to fabrication errors in the width. This can be understood because the continuity conditions for the fundamental TM mode mean that the effective index is mainly determined by the position of the horizontal

#154945 - $15.00 USD Received 19 Sep 2011; revised 21 Nov 2011; accepted 23 Nov 2011; published 3 Jan 2012

surfaces in the structure and hence varies rapidly with film thickness. On the other hand the TM mode index is much less sensitive to the positions of the vertical surfaces leading a low sensitivity to waveguide width.

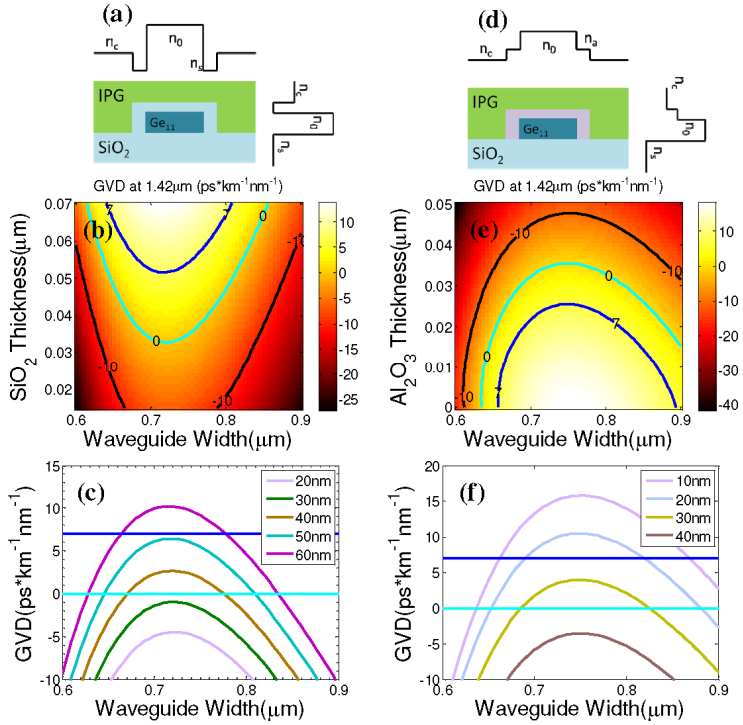

Fig. 6. (a) Waveguide with an inserted layer of SiO_2. (b) GVD as a function of SiO_2 layer thickness and waveguide width with 0.64 μm initial film thickness. (c) GVD as a function of waveguide width with 0.64μm initial film thickness. (d) Waveguide with an inserted layer of Al_2O_3. (e) GVD as a function of Al_2O_3 layer thickness and waveguide width with 0.61 μm initial film thickness. (f) GVD as a function of waveguide width with 0.61 μm initial film thickness.

By studying Fig. 5(a), we can see there is no region that lies close to the zero-dispersion contour that is sufficiently tolerant to fabrication errors in both film thickness and waveguide width to allow the reliable manufacture of a low dispersion structure. As a result we need a new approach. We started by choosing region II for our initial structure. What is now needed is a method to compensate fabrication errors in film thickness and which allows the maximum GVD to be tuned post fabrication to between zero and 7 $ps{\cdot}km^{-1}nm^{-1}$.

We found that it could be achieved by inserting a uniform layer between the waveguide and the upper cladding so that the GVD could be tuned by varying the thickness of this additional layer. Two variations on this procedure are shown in Figs. 6(a), (b) and (c) where a silica layer was inserted to compensate for too thick a waveguide, and Figs. 6(d), (e), (f) where the waveguide was too thin and an alumina layer was inserted. Figure 6(a) shows the structure and index profile when using the silica layer. In Fig. 6(b), we calculated the GVD as a function of waveguide width and SiO_2 layer thickness assuming the waveguide thickness was 0.64 μm: +15 nm greater than the target thickness of 0.625 μm. In this case the GVD was originally –6 $ps{\cdot}km^{-1}nm^{-1}$. By inserting SiO_2 whose refractive index is lower than that of IPG cladding (1.52), the GVD increases from negative to positive values as with the thickness of the SiO_2 layer is increased. This indicated that the positive errors in the film thickness could be compensated by tuning the TM mode index using the silica layer. More details can be seen in Fig. 6(c) which demonstrates that using a 40 nm SiO_2 layer, the maximum of GVD value

#154945 - $15.00 USD Received 19 Sep 2011; revised 21 Nov 2011; accepted 23 Nov 2011; published 3 Jan 2012

has increased to 2.5 ps·km^{-1}nm^{-1} with over 80 nm tolerance to waveguide width for GVD between zero and 2.5 ps·km^{-1}nm^{-1}. With a 50 nm SiO_2 layer, the peak value of GVD increased to 6.5 ps·km^{-1}nm^{-1} and over 150 nm tolerance to waveguide width is achieved.

When the waveguide is too thin, for example 0.61 μm corresponding to −15 nm error relative to the targeted film thickness of 0.625 μm, the peak value of GVD far exceeds the maximum of 7 ps·km^{-1}nm^{-1}. According to Figs. 6(d) and (e), however, inserting a layer of Al_2O_3 whose refractive index is higher than that of the IPG cladding again allows the TM mode index to be tuned but in this case the GVD decreases as the thickness of the Al_2O_3 layer increases thereby compensating the errors caused by the thinner waveguide film. From Fig. 6(f), using 30 nm of Al_2O_3 reduced the peak dispersion to 4 ps·km^{-1}nm^{-1} and achieves over 130 nm tolerance to waveguide width.

Although this method can be used to compensate the fabrication error in $Ge_{11.5}$ waveguide thickness, this additional layer also has an error tolerance in its thickness. According to Figs. 6(b) and (e), we found that SiO_2 and Al_2O_3 layers need to be controlled to a tolerance of 15 nm and 8 nm respectively. The reason that Al_2O_3 has poorer fabrication error tolerance than SiO_2 is because the refractive index contrast between Al_2O_3 and IPG is much larger than that between SiO_2 and IPG leading a more rapid change of GVD with Al_2O_3 layer thickness. In fractional terms the thickness of either film has to be controlled to 20–30% which is technologically feasible using various different deposition processes.

For example, although the fabrication tolerance on the thickness of the SiO_2 or Al_2O_3 layers is small in absolute terms, they can be realized using atomic layer deposition (ALD). This technology allows film thickness to be controlled on the atomic scale and produces conformal coatings on structured surfaces [16]. ALD is available for a variety of materials including Al_2O_3, SiO_2, ZnO, etc. It is a surface self-limiting process where film growth terminates after deposition of a single layer of atoms. Hence it allows the growth of thin amorphous layers with nanometer precision. ALD, therefore, allows us to add a layer of SiO_2 or Al_2O_3 with accurately controlled thickness to modulate the refractive index profile of waveguide cladding as illustrated in Fig. 6. This should allow us to fabricate a waveguide with near-zero anomalous dispersion insensitive to the waveguide width by compensating the fabrication errors in film thickness with a high precision process. This method relies on accurate measurement of the waveguide thickness post deposition and the choice of a target thickness that allows either SiO_2 or Al_2O_3 be deposited by ALD to tune the dispersion in the appropriate direction. In our experience optical profilometry can achieve the required measurement accuracy in films after processing.

4. Conclusion

We have designed $Ge_{11.5}As_{24}Se_{64.5}$ glass nanowire waveguides with near-zero anomalous dispersion at 1420 nm that can be made tolerant to fabrication errors through the use of a double-cladding. This structure leads to a large tolerance to waveguide width of 80–170 nm and utilizes a SiO_2 or Al_2O_3 layer deposited by atomic layer deposition to compensate any fabrication errors in the waveguide thickness. According to our analysis, nanowires with near-zero anomalous dispersion can generate correlated photon-pairs by spontaneous four-wave mixing with over 17 THz detuning from the pump in a region where Raman noise is absent. In these regions the photon pair correlation is predicted to be >100; the figure of merit >10; and source brightness of ~8×10^8 pairs/s. By fabricating a waveguide with group velocity dispersion of <5 ps·km^{-1}nm^{-1} these parameters are maintained over a bandwidth of >15 THz.

Acknowledgments

This research was conducted by the Australian Research Council Centre of Excellence for Ultrahigh Bandwidth Devices for Optical Systems (project number CE110001018).

#154945 - $15.00 USD Received 19 Sep 2011; revised 21 Nov 2011; accepted 23 Nov 2011; published 3 Jan 2012